ORNL/TM-2021/2159

Report on FY 2021 Testing in Support of the Development of EPP Plus SMT Design Method at ORNL

Yanli Wang
Peijun Hou
Mark C Messner
Robert I. Jetter
T.-L. Sham

Approved for public release.
Distribution is unlimited.

September 2021

OAK RIDGE National Laboratory

ORNL IS MANAGED BY UT-BATTELLE LLC FOR THE US DEPARTMENT OF ENERGY

ORNL/TM-2021/2159

Materials Science and Technology Division

REPORT ON FY 2021 TESTING IN SUPPORT OF THE DEVELOPMENT OF EPP PLUS SMT DESIGN METHOD AT ORNL

Yanli Wang
Peijun Hou[1]
Mark C Messner[2]
Robert I. Jetter[3]
T.-L. Sham[4]

[1] Imtech Corporation, Knoxville
[2] Argonne National Laboratory
[3] RI Jetter Consulting
[4] Idaho National Laboratory

Date Published: September 2021

Prepared by
OAK RIDGE NATIONAL LABORATORY
Oak Ridge, TN 37831-6283
managed by
UT-BATTELLE, LLC
for the
US DEPARTMENT OF ENERGY
under contract DE-AC05-00OR22725

CONTENTS

LIST OF FIGURES v
LIST OF TABLES vi
ABBREVIATIONS vii
ACKNOWLEDGMENTS ix
ABSTRACT 1
1. BACKGROUND 1
2. MATERIAL AND EXPERIMENT 2
3. CREEP-FATIGUE DATA AT LOW STRAIN RANGES 4
   3.1 LIMITATIONS ON CF DATA AT LOW STRAIN RANGES 4
   3.2 RESULTS ON STANDARD CF 5
   3.3 SMT-BASED TEST DATA AT LOW STRAIN RANGE 6
4. CF LIFE-PREDICTION METHODS USING AVAILBLE CF DATA 8
   4.1 CREEP DAMAGE ACCUMULATION METHOD 9
      4.1.1 Creep Damage Calculation of CF Tests 9
      4.1.2 Creep Damage Analysis on CF Failure Data at Low Strain Ranges 10
      4.1.3 Creep Damage Method for CF Life Prediction 11
   4.2 Dissipated work-based METHOD 13
      4.2.1 Dissipated Work Calculation of CF Tests 13
      4.2.2 Dissipated Work Calculation and CF Life Prediction at Low Strain Ranges 14
   4.3 COMPARISON OF CF CYCLES USING DIFFERENT EXTRAPOLATION METHODS 17
5. TESTING IN GENERATING CF DESIGN CURVES AT LOW STRAIN RANGES 18
   5.1 BLOCK STRAIN RANGE CF TESTING 18
   5.2 PRELIMINARY CF DESIGN CURVES 20
   5.3 EXPERIMENTS IN VALIDATING THE CF DESGIN CURVE 21
6. SUMMARY 23
REFERENCES 24

LIST OF FIGURES

Figure 1. Standard fatigue and CF specimen geometry at Oak Ridge National Laboratory (ORNL). 3
Figure 2. Strain-controlled CF straining profile for one cycle. 4
Figure 3. (a) Maximum and minimum stresses and (b) strain ranges as a function of applied cycles for standard CF R13BC3 with 20 s hold time and R13TC6 with 120 s hold time. 5
Figure 4. Representative hysteresis loops for (a) R13BC3 with a 20 s hold time and (b) R13TC6 with a 120 s hold time. 6
Figure 5. Stresses at the beginning and end of the holding segment for R13BC3 with a 20 s hold time and R13TC6 with a 120 s hold time. 6
Figure 6. (a) Maximum and minimum stresses and (b) strain ranges as a function of applied cycles for Type 1 SMT R16C3. 7
Figure 7. (a) Maximum and minimum stresses and (b) strain ranges (b) as a function of applied cycles for SBSMT SBA4-P16 and SBA7-P20. 8
Figure 8. Hysteresis loops at the midlife cycle in SBA4-P16 and SBA7-P20. 8
Figure 9. (a) Creep damage of individual cycles and (b) the accumulated creep damage as a function of applied cycles for R13BC3 and R13TC6. 10
Figure 10. (a) Creep damage of individual cycles and (b) the accumulated creep damage as a function of applied cycles for R16C3. 10
Figure 11. (a) Creep damage of individual cycles and (b) the accumulated creep damage as a function of applied cycles for SBA4-P16 and SBA7-P20. 11
Figure 12. (a) Extrapolation in creep damage increment and (b) the accumulated creep damage calculated based on the extrapolation as a function of the applied cycles. 12
Figure 13. Illustration of the dissipation work in one hysteresis loop. 13
Figure 14. (a) Dissipated work of each cycle and (b) the accumulated Dissipated work as a function of applied cycles for R13BC3 and R13TC6. 14
Figure 15. (a) Dissipated work of each cycle and (b) the accumulated dissipated work as a function of applied cycles for R16C3 14
Figure 16. (a) Dissipated work of each cycle and (b) the accumulated dissipated work as a function of applied cycles for SBA4-P16 and SBA7-P20. 15
Figure 17. (a) Tensile dissipated work of each cycle and (b) the accumulated tensile dissipated work as a function of applied cycles for R13BC3 and R13TC6. 15
Figure 18. (a) Tensile dissipated work of each cycle and (b) the accumulated tensile dissipated work as a function of applied cycles for R16C3. 16
Figure 19. (a) Tensile dissipated work of each cycle and (b) the accumulated tensile dissipated work as a function of applied cycles for SBA4-P16 and SBA7-P20. 16
Figure 20. CF life cycles prediction using creep damage accumulation, total dissipated work, and net tensile dissipated work methods on Alloy 617 subjected to low strain range CF at 950°C. 18
Figure 21. (a) Maximum and minimum stresses and (b) strain ranges as a function of applied cycles for the first five blocks of CF cycles. 19
Figure 22. (a) Dissipated work in each cycle and (b) the accumulated dissipated work as a function of applied cycles for the block strain range CF test. 20
Figure 23. Preliminary CF design curve for Alloy 617 at 950°C with the hold time of 100 s 21
Figure 24. Accumulated dissipated work as a function of applied cycles for (a) P10-10 and (b) R12TC4-05 along with the linear extrapolation curves. 22

LIST OF TABLES

Table 1. Chemical compositions of Alloy 617 plate with heat number 314626 (wt %). 3
Table 2. Results of standard CF testing for Alloy 617 with tension hold at 950°C. 5
Table 3. Results of previous SMT-based testing for Alloy 617 hold at 950°C 7
Table 4. Results of CF life prediction using creep damage accumulation method. 13
Table 5. Results of CF life cycles predicted using total dissipated work and tensile dissipated work methods. 17
Table 6. Block strain range CF at 950°C and results of predicted CF life cycles 19
Table 7. SMT-based CF testing for Alloy 617 at 950°C. 21

ABBREVIATIONS

ART	Advanced Reactor Technologies
ASME	American Society of Mechanical Engineers
B&PV	boiler and pressure vessel
CF	creep-fatigue
DOE	US Department of Energy
EPP	Elastic-Perfectly Plastic
ORNL	Oak Ridge National Laboratory
SBSMT	Single-Bar Simplified Model Test
SMT	Simplified Model Test

ACKNOWLEDGMENTS

This research was sponsored by the US Department of Energy (DOE) under contract no. DE-AC07-05ID14517 with Idaho National Laboratory, managed and operated by Battelle Energy Alliance; under contract no. DE-AC05-00OR22725 with Oak Ridge National Laboratory (ORNL), managed and operated by UT-Battelle LLC; and under contract no. DE-AC02-06CH11357 with Argonne National Laboratory, managed and operated by UChicago Argonne LLC. Programmatic direction was provided by the Office of Nuclear Reactor Deployment of the DOE Office of Nuclear Energy.

The authors gratefully acknowledge the support provided by Sue Lesica, federal manager of the Advanced Materials Advanced Reactor Technologies (ART) program; Diana Li, federal program manager of the ART Gas-Cooled Reactors (GCR) Campaign; and Gerhard Strydom of Idaho National Laboratory, national technical director of the ART GCR Campaign.

The authors also wish to thank ORNL staff members C. Shane Hawkins and Kelsey Hedrick for technical support and Edgar Lara-Curzio and Lianshan Lin for reviewing this report.

ABSTRACT

Experiments in support of the development of the integrated Elastic–Perfectly Plastic (EPP) plus Simplified Model Test (SMT) design methodology, referred to as the *EPP+SMT method*, continued in FY21. This report focuses on the methodology for developing the EPP+SMT creep-fatigue (CF) design curves at low strain ranges.

The creep damage-based method and dissipated work-based method were used to evaluate the available CF data at the low strain range region. A set of failure criteria were determined, and a simple extrapolation method was developed to predict the CF life cycles at low strain ranges that are not accessible by experiments due to the extraordinarily long failure times at the low strain region (thousands to hundreds of thousands of years) and the inability of the test machine to control these small strain ranges due to the signal to noise issues.

An experimental method with the concept of block-strain range CF testing was proposed to generate the information needed to extrapolate the CF design curves to low strain ranges. Based on this new testing approach, a preliminary EPP+SMT CF design curve was developed for Alloy 617 at 950°C with tension hold time of 100 s. The analysis in this report shows the potential of generating a set of EPP+SMT CF design curves with different hold times within a reasonable amount of time and testing effort.

Based on such a progress, a hold time extrapolation procedure for low strain ranges will be developed in FY22 and critical testing will be carried out to complete the development of the EPP+SMT CF design curves for Alloy 617.

1. BACKGROUND

Creep-fatigue (CF) at elevated temperatures is the most damaging structural failure mode. Significant efforts have been devoted to the elevated temperature code rule development in the American Society of Mechanical Engineers (ASME) *Boiler and Pressure Vessel Code* (Section III, Division 5, Subsection HB, Subpart B) in the last 40 years to ascertain conservative structural designs against CF failure. The current Subsection HB, Subpart B CF evaluation in the design procedure was established by (1) analytically obtaining a detailed stress-strain history, (2) comparing the stress and strain components with cyclic test results and deconstructed into stress and strain quantities to evaluate the creep damage and fatigue damage separately, and (3) recombining the results to obtain a damage function in the form of the CF damage diagram. The deconstruction and recombination stress and strain quantities present difficulties in evaluating test data and determining cyclic damage in design. The uncertainties in these steps lead to the use of overly conservative approach in the current CF procedure.

The integrated Elastic–Perfectly Plastic (EPP) plus Simplified Model Test (SMT) design methodology, referred to as the *EPP+SMT method*, is an alternative CF evaluation methodology. The concept is to incorporate the SMT CF test data-based approach into the EPP methodology to avoid evaluating creep and fatigue damage separately. It greatly simplifies the evaluation procedure for elevated temperature cyclic service. In the SMT-based approach, the primary point is that it no longer requires the damage interaction, or damage diagram, and the combined effects of creep and fatigue are accounted for in the SMT test data. The SMT specimens are designed to replicate or bound the stress and strain redistribution that occurs in actual components when loaded in the creep regime. On the other hand, the EPP methods greatly simplify the design evaluation procedure by eliminating the need for stress classification, which is the basis of the current simplified design rules. The goal of this EPP+SMT methodology is to maximize the advantages of EPP methods and the SMT CF evaluation approach. The EPP+SMT method also aims to minimize the over-conservatism in the existing CF evaluation procedure by using the damage

interaction diagram while properly accounting for enhanced creep damage around localized defects and stress risers.

A detailed plan was developed and revised for the development of this EPP+SMT methodology (Wang et al. 2016a, 2016b, 2017a, 2018, 2019; Messner 2018). The development of SMT-based design curves requires experimental data, and the parameters to be considered include elastic follow-up factor, strain range, loading rate, test temperature, hold time, and primary load. In the original SMT key feature testing methods, the elastic follow-up factor was achieved by sizing the length and area ratios of the driver section to the test section. Achieving the requisite representation of creep damage characteristics via key featured SMT, particularly at very high temperatures, involves specimen configurations that are both costly and beyond the limits of test control and stability (Wang et al. 2013, 2014, 2015, 2016a, 2017b, 2017c). Although key featured SMT testing is crucial in verifying the SMT-based design methodology, it is impractical for use in generating data for SMT-based design curves.

Significant progress was made in developing SMT experimental techniques by Wang et al. (2018, 2019, 2020). In particular, the newly developed single-bar SMT (SBSMT) test method and test protocol overcome many challenges associated with conducting SMT key feature experiments and enable the evaluation of the effect of elastic follow-up by using a standard CF specimen without the need for specialized instrumentation and specimen design. In FY19, Wang et al. (2019) demonstrated the SBSMT method on Alloy 617, SS316H, and Grade 91 by testing at high temperatures and successfully showed the flexibility of generating SMT-based failure data with a wide range of elastic follow-up values from 1 to 12. The SBSMT test method significantly simplifies the procedure for generating SMT test data and allows SMT-based design method development to advance rapidly. In FY20, Wang et al. (2020, 2021) extended the SBSMT method to internal pressurized tubular specimens at 950°C on Alloy 617. The sustained primary load was introduced by the internal pressure. The test results from this study along with the original SMT data on Alloy 617 demonstrate that although internal pressure is within the allowable stress limit per ASME Section III, Division 5, Code Case N-898, the SMT CF cycles to failure were reduced for the cases tested with primary-pressure load. The reduction of SMT CF life because of primary load was found to depend on strain ranges and elastic follow-up. Approaches to handle the primary-load effect on SMT design curves are discussed in Barua et al. (2020, 2021), and the EPP strain range analysis procedure naturally captures the primary pressure effect. Barua et al. (2020, 2021) also demonstrated that the EPP+SMT methodology is much simpler to execute than conventional CF damage analyses through multiple example problems.

The remaining critical factors in finalizing the SMT-based design curves are the methods for extrapolating the design curves to the low strain range region and with longer hold times that are prototypical of plant operations. During this reporting period, standard CF tests were performed on Alloy 617 at 950°C at low strain ranges of 0.18 and 0.17%. The results and previous SMT tests with low strain ranges were used to evaluate the two methods for the extrapolation into lower strain ranges and long hold times (i.e., creep damage rate method and the dissipated work-based method). Although there are limited data available, the analysis in this report showed promising solution in finalizing the SMT-based design curves.

2. MATERIAL AND EXPERIMENT

The Alloy 617 specimens were machined from the Alloy 617 plate with heat number 314626 from ThyssenKrupp VDM USA Inc, supplied to support this research by Idaho National Laboratory. The plate has a nominal thickness of 38 mm. The chemical composition of the plate is listed in Table 1.

Table 1. Chemical compositions of Alloy 617 plate with heat number 314626 (wt %).

C	S	Cr	Ni	Mn	Si	Mo	Ti	Cu	Fe	Al	Co	B
0.05	<0.002	22.2	54.1	0.1	0.1	8.6	0.4	0.04	1.6	1.1	11.6	<0.001

The specimen geometry used in this study for standard CF tests is shown in Figure 1. The specimen has a gage diameter of 6.35 mm and a gage length of 19.05 mm. The CF testing followed ASTM E2714-13 standard (ASTM 2013) under strain-controlled mode. The specimen longitudinal direction is oriented along the rolling direction of the plate. All the specimens were tested in the as-received condition.

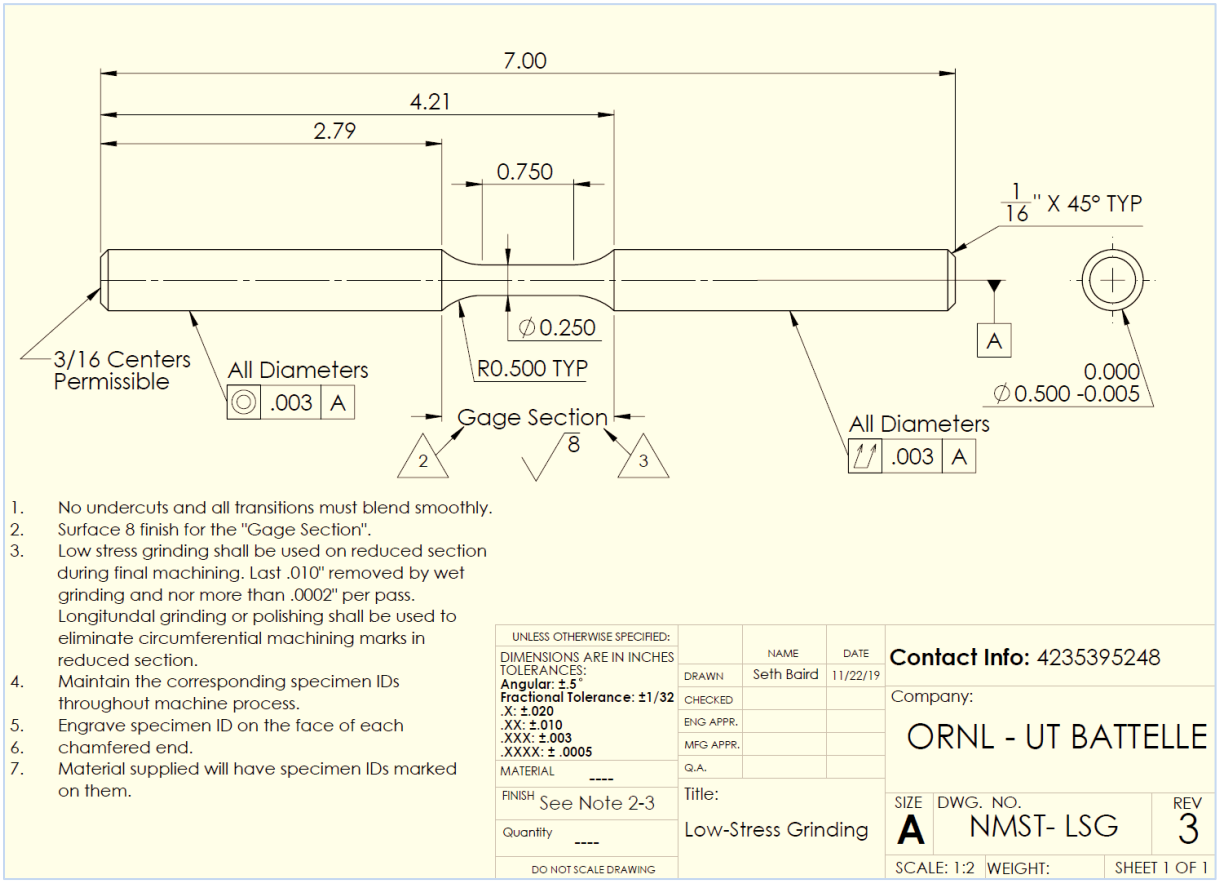

Figure 1. Standard fatigue and CF specimen geometry at Oak Ridge National Laboratory (ORNL). Dimensions are in inches.

The straining profile for standard strain-controlled CF is shown schematically in Figure 2. The hold-time segment is applied to the maximum tensile strain amplitude for CF testing. The straining profile is a fully reversed profile (i.e., with a nominal straining ratio of $R = -1$). The nominal strain rate is 1E-3/s. The control extensometer has a nominal gage length of 12.7 mm.

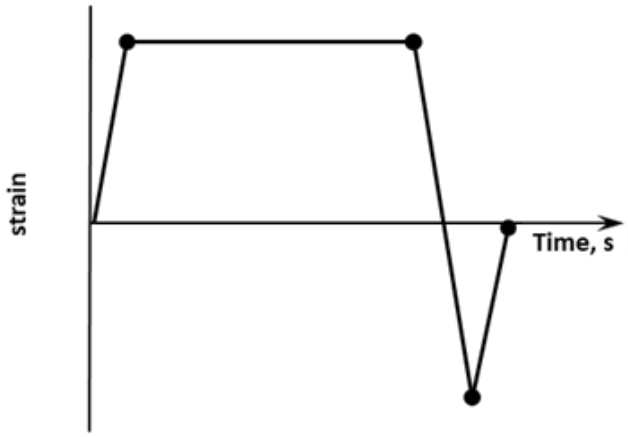

Figure 2. Strain-controlled CF straining profile for one cycle.

There are ongoing SBSMT tests with a designed elastic follow-up factor of 3 on Alloy 617 at 950°C with a tension hold time of 600 s. The test specimen geometry and the test setup are the same as the standard CF (Wang et al. 2019).

Previous SMT-based CF test results at low strain ranges at 950°C on the same heat of Alloy 617 plate (heat 314626) were added to the analysis provided in the following sections. The details of the experimental procedure are explained in the previous report (Wang et al. 2020, 2019, 2018, 2016a, 2013).

3. CREEP-FATIGUE DATA AT LOW STRAIN RANGES

3.1 LIMITATIONS ON CF DATA AT LOW STRAIN RANGES

To the best of the authors' knowledge, uniaxial strain-controlled CF failure data exist only at strain range of ≥0.3%. There are two main practical reasons for the lack of CF data at low strain ranges. First, the noise-to-signal ratio at the low strain ranges is high for all standard high-temperature CF testing instrumentation. The commonly used extensometers, load cells, temperature controls, and servo hydraulic machines all have limitations in their accuracy. For example, per ASTM E2714-13, the axial force measured during the test is required to have reading accuracies >1%, the control stability should be such that the maximum and minimum limits of the control variable are maintained within 1% of its range, and the heating source shall be such that the test specimen can be uniformly heated to the specified temperature with an indicated temperature gradient across the gage section that is less than or equal to the greater of 2°C or 1% of the nominal test temperature throughout the duration of the test. These specifications depict the capability of modern instrumentation with good quality. However, looking at the testing at high temperatures with 950°C as an example, modern instrumentation allows the test temperature variation within 1% of the target temperature, i.e., 9.5°C, per the ASTM standard. Thus, the temperature variation allows a thermal strain of 1.6E-4, corresponding to 10% variation in the controlling strain for testing at 0.16%, or much higher ratio for lower strain ranges. And this 10% of variation is in addition to the 1% noise in the strain and load signals. Second, it is impractical to produce failure data at very low strain ranges because of the long test duration. For example, at strain range of 0.2% with 10 min tensile hold time, it takes ~17,000 h to produce one CF failure data point with cycles to failure of 1E5. The long test duration makes it impossible to generate CF design curves based on CF testing failure data at low strain ranges. The same issue of unreasonably long test duration for CF failure data is with long hold times. For example, for a typical operation hold time of 1,000 h, a CF test with failure cycles of 10 cycles will require a testing time of more than 1 year. At strain ranges much lower 0.3%, assuming the

failure cycles to be on the order of 1E4 or 1E5 cycles, based on available short hold time data, it leads to test times of 1,140 to 11,400 years. Thus, a methodology in the extrapolation of the CF cycles at the low strain ranges and longer hold time is necessary.

This section analyzes the available CF failure data at low strain ranges generated under the Advanced Reactor Technologies (ART) Program. These data provide critical information on the validation of the methods for CF life prediction at low strain ranges.

3.2 RESULTS ON STANDARD CF

Standard CF experiments were performed on two Alloy 617 specimens at 950°C: R13BC3 with 20 s tension hold time at peak tensile strain amplitude with nominal strain range of 0.18% and R13TC6 with 120 s tension hold time at nominal strain range of 0.17%. The maximum and minimum stresses and the strain ranges are shown in Figure 3. For R13BC3, the noticeable changes in the maximum and minimum stresses at about 100 cycles are due to the experimental restart, and the exact initial strain range could not be maintained. The maximum stresses are higher in the R13BC3 with a 20 s hold time, even when the strain range upon restart was slightly lower than the initial strain range. The strain ranges in R13TC6 were controlled with relatively more stability. The noise in the control strain range was about ±0.015%, which is expected at this level of low strain range. The results of these two standard CF tests are summarized in Table 2.

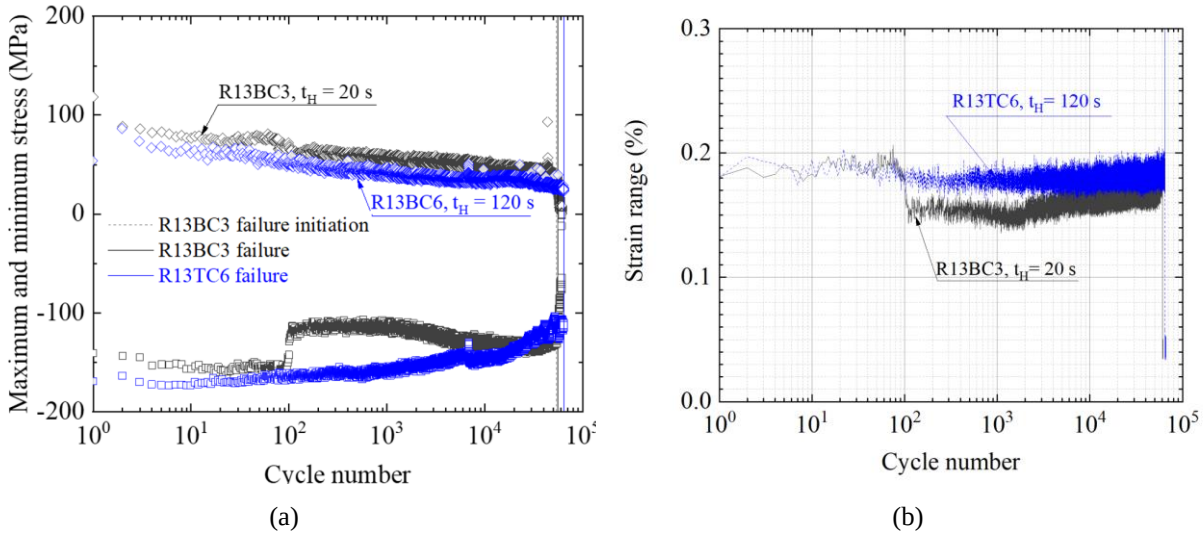

Figure 3. (a) Maximum and minimum stresses and (b) strain ranges as a function of applied cycles for standard CF R13BC3 with 20 s hold time and R13TC6 with 120 s hold time.

Table 2. Results of standard CF testing for Alloy 617 with tension hold at 950°C.

Specimen ID	Average strain range (%)	Test temperature (°C)	Holding segment	Hold time (s)	Cycles to failure
R13BC3	0.18	950	Tension	20	55,289
R13TC6	0.17	950	Tension	120	64,659

Representative hysteresis loops (i.e., first, second, third, tenth, and midlife cycles) for both tests are presented in Figure 4. Although the stress and strain signals are noisy, the plots show that R13TC6

generally has wider hysteresis loops compared with the R13BC3 because of the longer hold time applied at peak tension strain. The longer hold time allowed for a larger amount of stress relaxation, which widens the hysteresis loops. To better illustrate the hold time effect on the stress relaxation behavior for these two tests, Figure 5 compares the stresses at the beginning and end of the hold as a function of the applied cycles. The comparison shows that the difference between stresses at the beginning and end of the hold are consistently larger in R13TC6 with a longer hold time of 120 s.

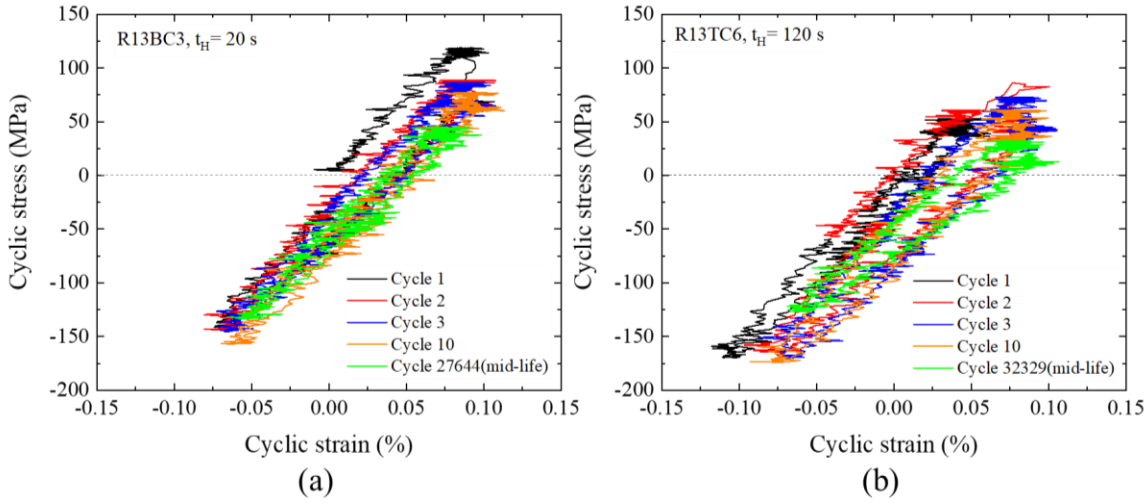

Figure 4. Representative hysteresis loops for (a) R13BC3 with a 20 s hold time and (b) R13TC6 with a 120 s hold time.

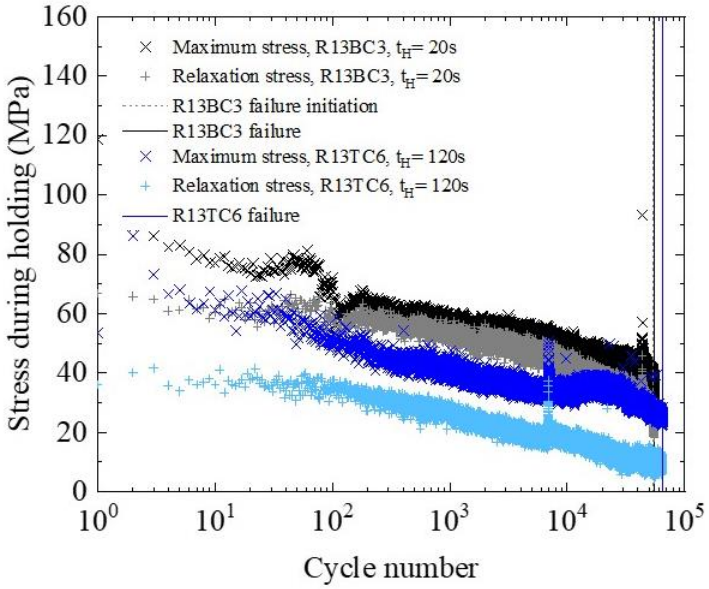

Figure 5. Stresses at the beginning and end of the holding segment for R13BC3 with a 20 s hold time and R13TC6 with a 120 s hold time.

3.3 SMT-BASED TEST DATA AT LOW STRAIN RANGE

In previous CF testing data on this same heat of Alloy 617 at 950°C under the Advanced Reactor Technologies (ART) program, there are failure data from SMT-based CF tests at low strain ranges. These

available SMT-based tests are listed in Table 3, and the data are re-analyzed in this report to extract relevant information for prediction of CF life cycles. These three tests were tested to failure, and the strain ranges were less than 0.3%, so they are valuable data points in support of developing the methods for predicting CF life cycles at low strain ranges.

Table 3. Results of previous SMT-based testing for Alloy 617 hold at 950°C.

Test ID	Testing type	Specimen geometry	Initial stable strain range (%)	Elastic follow-up factor	Tension hold time (s)	Cycles to failure
R16C3[1]	Type 1 SMT	Type 1 solid specimen	0.16	3.5	180	10,766
SBA4-P16[2]	SBSMT	Tubular SMT specimen with internal pressure of 2 psi	0.18	6.0	600	3,641
SBA7-P20[2]	SBSMT	Tubular SMT specimen with internal pressure of 2 psi	0.25	2.0	600	3,224

[1] The Type 1 SMT test is described in Wang et al. (2016a).
[2] The SBSMT tests on these tubular shaped specimens are described in Wang et al. (2020).

The maximum and minimum stresses and strain ranges for Type 1 SMT R16C3 with tension hold times of 180 s are presented in Figure 6. The average strain ranges are 0.16%. There were multiple interruptions for this test at cycles of ~300, which caused the discontinuities in the plots. The unintentional interruptions are associated with operational factors, such as heater failure, electricity outage, or failure to maintain the temperature gradient. Although these interruptions are unideal for the test data, they are inevitable for long-duration testing. The restart of the test had a cooldown and reheat thermal cycle effect. The nominal elastic follow-up factor for the Type 1 SMT at 950°C is 3.5. More details on the R16C3 SMT testing can be found in Wang et al. (2016a).

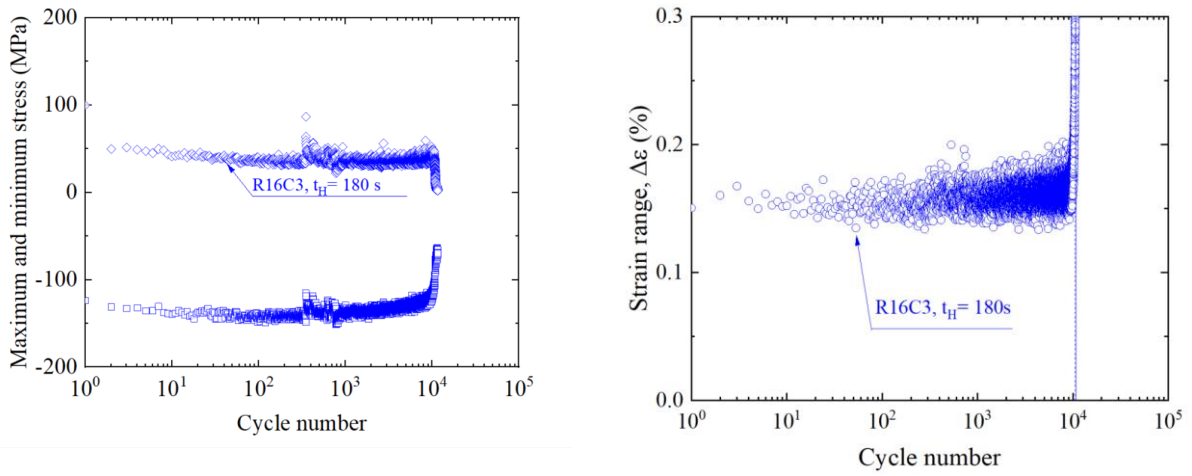

(a) (b)

Figure 6. (a) Maximum and minimum stresses and (b) strain ranges as a function of applied cycles for Type 1 SMT R16C3.

Additionally, the results of two SBSMT tests with tubular-shaped specimen geometry with an internal pressure of 2 psi at 950°C—SBA4-P16 and SBA7-P20 from Wang et al. (2020)—are presented in this report. The nominal elastic follow-up factors were 6.0 and 2.0 for SBA4-P16 and SBA7-P20,

respectively. Both cases had a peak tension hold time of 600 s. Figure 7 presents the maximum and minimum stresses and the strain ranges of these two tests. The initial stabilized strain ranges are 0.18% for SBA4-P16 and 0.25% for SBA7-P20, respectively. The hysteresis loops of the midlife cycles for SBA4-P16 and SBA7-P20 are presented in Figure 8. The slope of the relaxation segments of the hysteresis loop are different for these two tests because of the different designed elastic follow-up factors. The stress relaxation was slower in SBA4-P16 than in SBA4-P16 at the 600 s hold time because of its higher elastic follow-up factor of 6.0.

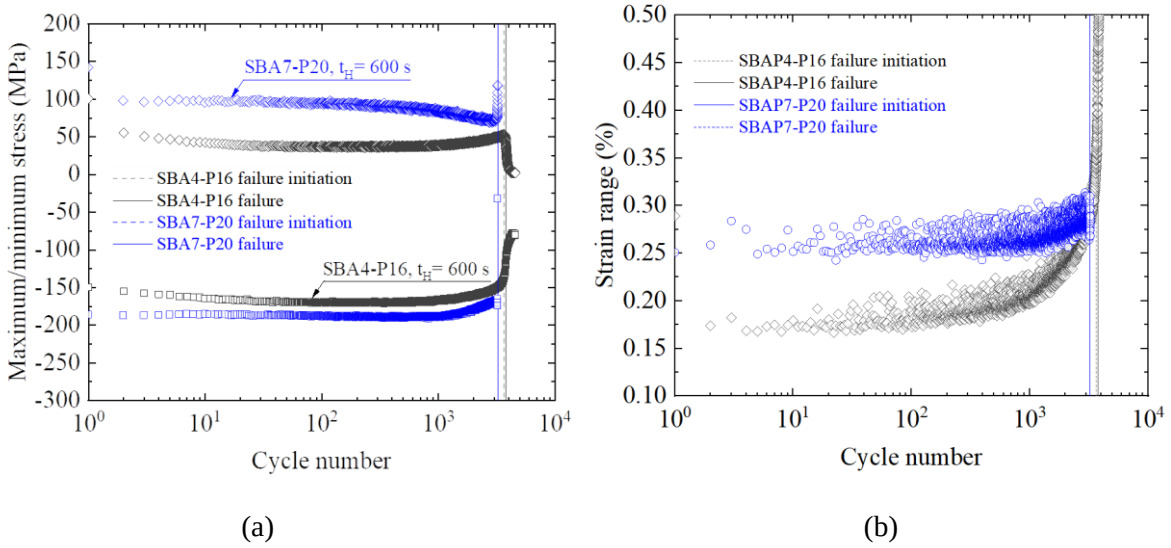

(a) (b)

Figure 7. (a) Maximum and minimum stresses and (b) strain ranges (b) as a function of applied cycles for SBSMT SBA4-P16 and SBA7-P20.

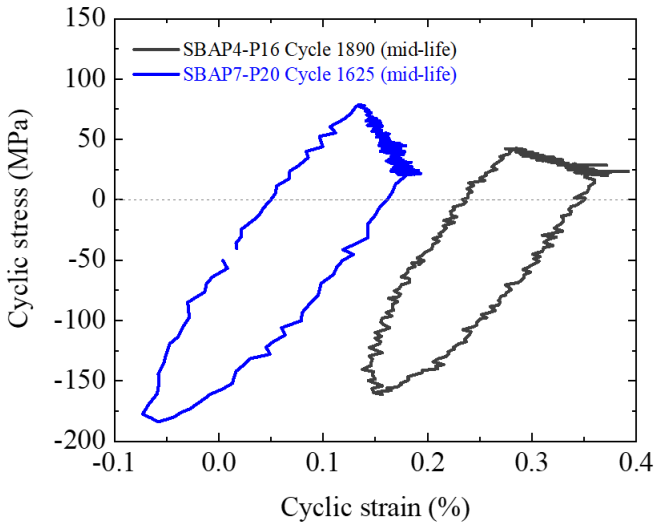

Figure 8. Hysteresis loops at the midlife cycle in SBA4-P16 and SBA7-P20.

4. CF LIFE-PREDICTION METHODS USING AVAILBLE CF DATA

In the literature, there are several methods in the perdition of the CF life cycles at the low strain ranges (Hales 1980, Mason and Zab 1977). In this section, the test data from low strain ranges are used to

evaluate two methods for CF life prediction: the creep damage accumulation method and dissipated work-based method.

4.1 CREEP DAMAGE ACCUMULATION METHOD

4.1.1 Creep Damage Calculation of CF Tests

For specimens tested under CF at low strain ranges, the cyclic life is assumed to be dominated by the creep damage (Hales 1980). The available standard CF test results in this study—R13BC3 with 20 s tension at nominal strain range of 0.18% and R13TC6 with 120 s tension hold time at nominal strain range of 0.17%—showed fatigue damage of less than 10%. The fatigue damage is defined as the ratio of the cycles to failure of the CF tests to those of the pure fatigue tests at the same strain ranges. In the following analysis, the creep damage-based calculation is used to evaluate the failure life at low strain ranges.

A conventional approach estimating the creep damage is applied in which the time fraction during the hold segment is used as a measure of creep damage. The creep damage of the αth cycle, D_α, is given as:

$$D_\alpha = \int_0^{t_H} \frac{1}{t_r} dt, \tag{1}$$

where t_H is the hold time, and t_r is the creep rapture time at each stress level. The accumulated creep damage over *N* cycles, D, is expressed as the linear summation of the creep damage over the test cycles:

$$D = \sum_1^N D_\alpha = \sum_1^N \int_0^{t_H} \frac{1}{t_r} dt. \tag{2}$$

The creep rupture time, t_r, can be derived from the Larson-Miller relationship at test temperature, T, and applied stress, σ:

$$LMP = T(C + log_{10} t), \tag{3}$$

$$LMP = a_0 + a_1 log_{10} \sigma, \tag{4}$$

where *LMP* is the Larson-Miller parameter, *C* is the Larson-Miller constant, and a_0 and a_1 are fitting parameters. The units of time, temperature, and stress in the Larson-Miller relation are hour, kelvin, and MPa, respectively. The fitting parameters, a_0 and a_1, and the Larson-Miller constant, *C*, used in the present report were obtained from Wright et al. (2016), where $a_0 = 32976.41$, $a_1 = -5908.10$, and $C = 16.73$.

The stress relaxation curves are fitted according to the power law formula and are expressed as a function of the hold time for each cycle:

$$\sigma = b_0 (t + t_0)^{b_1} \tag{5}$$

where σ is the stress during the holding segment, b_0 and b_1 are the fitting parameters for each cycle, and t_0 is set to 2 s in this analysis. Note that t_0=2 s is used here to offset the time at the beginning of the hold segment to capture the maximum stress during the cycle due to the noise, and this is not supposed to be universally applicable for all other CF test conditions.

4.1.2 Creep Damage Analysis on CF Failure Data at Low Strain Ranges

The creep damage of the individual cycles calculated from the hold time segment and the accumulated creep damage for the two standard CF tests, R13BC3 and R13TC6, are presented in Figure 9. Although R13BC3 was tested with a shorter hold time of 20 s, the calculated creep damage was much larger for each cycle because of its higher stress levels, thus resulting in higher accumulated creep damage as a function of applied cycles. The calculated accumulated creep damage was 0.23 for R13TC6, and 1.16 for R13BC3.

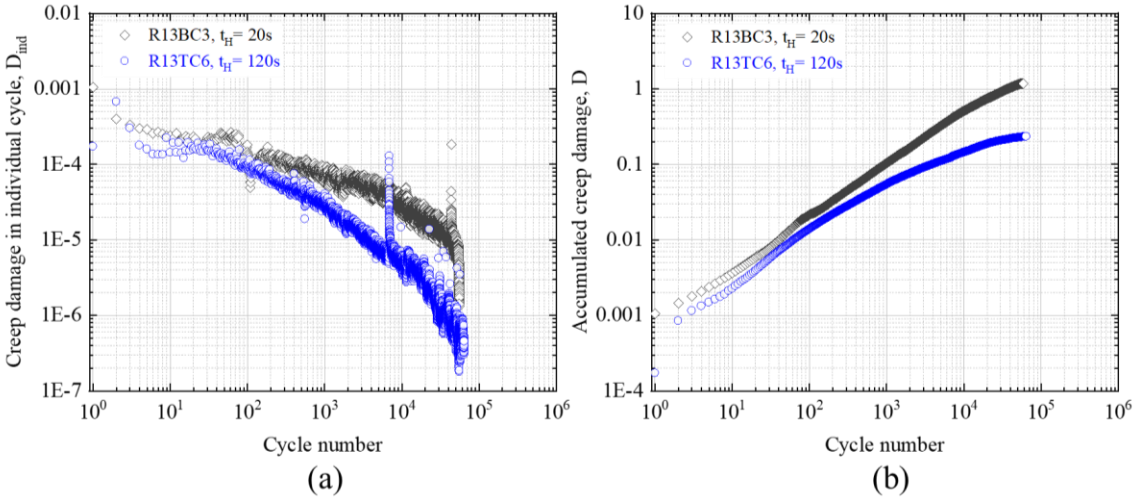

Figure 9. (a) Creep damage of individual cycles and (b) the accumulated creep damage as a function of applied cycles for R13BC3 and R13TC6.

Figure 10 presents the individual and accumulated creep damage for Type 1 SMT R16C3. This test had an initial strain range of 0.16% and a tension hold time of 180 s. The accumulated creep damage upon failure for R16C3 is approximately 0.21. The interruptions for this test at cycles of ~300 increased the creep damage at the beginning of the cycles.

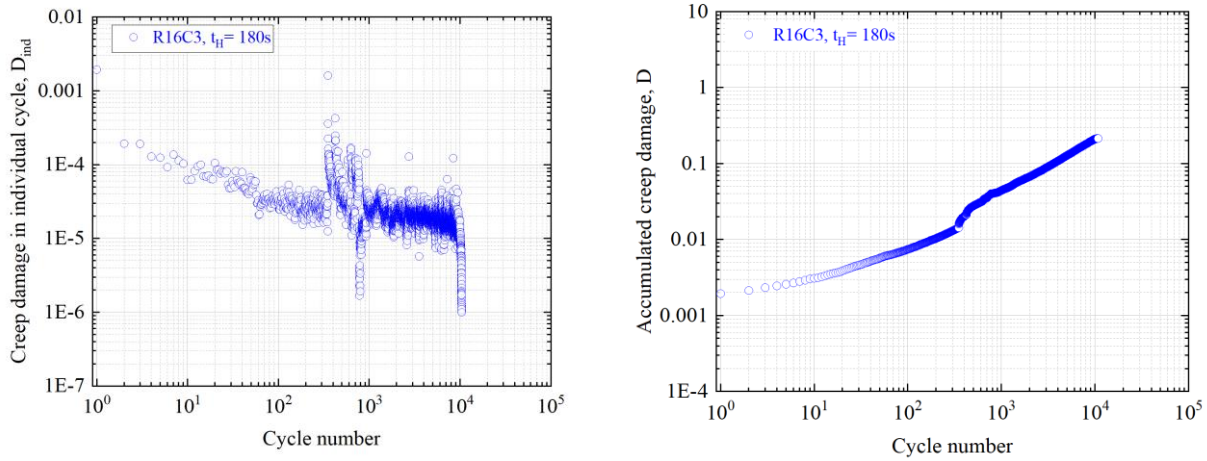

Figure 10. (a) Creep damage of individual cycles and (b) the accumulated creep damage as a function of applied cycles for R16C3.

Figure 11 shows the results of the creep damage calculation for SBA4-P16 with an elastic follow-up factor of 6.0 and SBA7-P20 with and elastic follow-up factor of 2.0. Because of the larger strain ranges, the SBA7-P20 shows higher creep damage for the individual cycles and faster creep damage accumulation rate, although it had smaller elastic follow-up factor of 2.0. The accumulated creep damage is approximately 0.25 for SBA4-P16 and 0.59 for SBA7-P20.

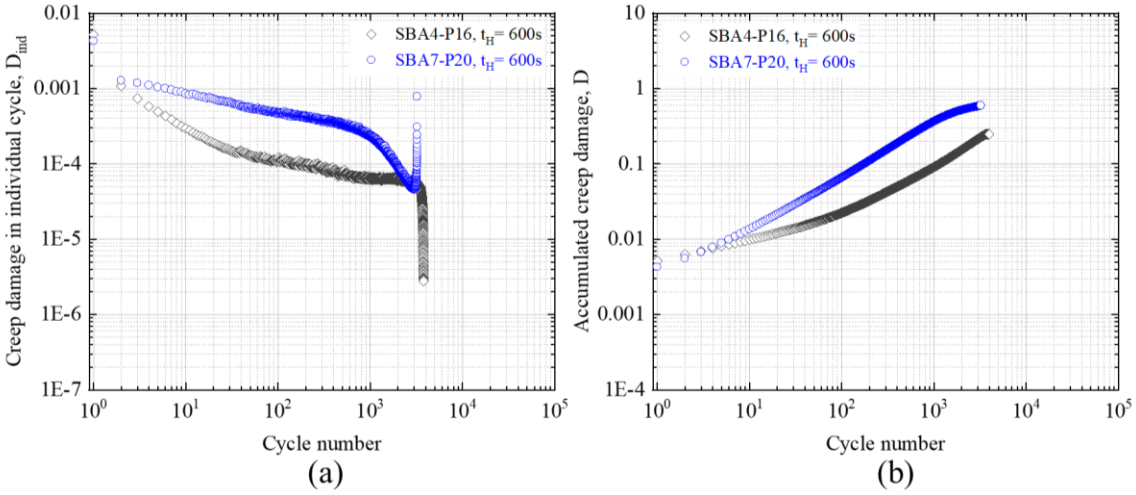

Figure 11. (a) Creep damage of individual cycles and (b) the accumulated creep damage as a function of applied cycles for SBA4-P16 and SBA7-P20.

4.1.3 Creep Damage Method for CF Life Prediction

From the aforementioned creep damage calculations on the available CF test data in the low strain range region, the following findings can be made. First, CF data at low strain ranges are very limited. The specimens tested to failure usually have a much higher noise-to-signal ratio than those at higher strain ranges. Second, the accumulated creep damage in these limited number of tests at low strain ranges are dependent on strain ranges, hold times, and elastic follow-up effects. Third, the lower bound of the accumulated creep damage was about 0.2 based on the five tests at low strain ranges. Finally, SMT-based CF tests had the advantage of shorter test duration due to the elastic follow-up-induced faster creep damage for tests with the same strain levels; however, the strain ranges measured in the test section are not constant.

Knowing the challenges in the low strain range CF tests and the aforementioned findings, the following explains a potential method for CF life cycle prediction at low strain ranges by using the creep damage-based concept. This approach is similar to what was proposed by Hales (1980), and the creep damage is deemed to be the comminating damage mechanism at the low strain range region. In this study, two assumptions were made based on the aforementioned analysis: (1) the accumulated creep damage for the CF tests at low strain ranges at 950°C for Alloy 617 has a lower bound value of 0.2, and (2) after the initial cycles, the creep damage as a function of the applied cycle has a simple linear trend in a log-log scale before failure initiation. In this study, the calculated creep damage of cycles 100–200 is used for the trend line extrapolation to cycles beyond 200. The results are presented in Figure 12a.

The initial cycles before establishing the trend line were only two to three cycles for three tests (i.e., SBA7-P20, R16C3, and R13BC3) and about 20 cycles for R13TC6. The test SBA4-P16 showed continuous change against linear extrapolation with more applied cycles, likely because its elastic follow-up factor of 6.0 was too high to represent the typical CF test behaviors at lower strain ranges. The accumulated creep damage curves calculated from the trend line for each test are presented in Figure 12b

along with the actual accumulated creep damage. The results show that the trend line curves capture the experimental creep damage data reasonably well, except for two cases: SBA4-P16 with an elastic follow-up factor that was too large and R16C3 with multiple interrupted.

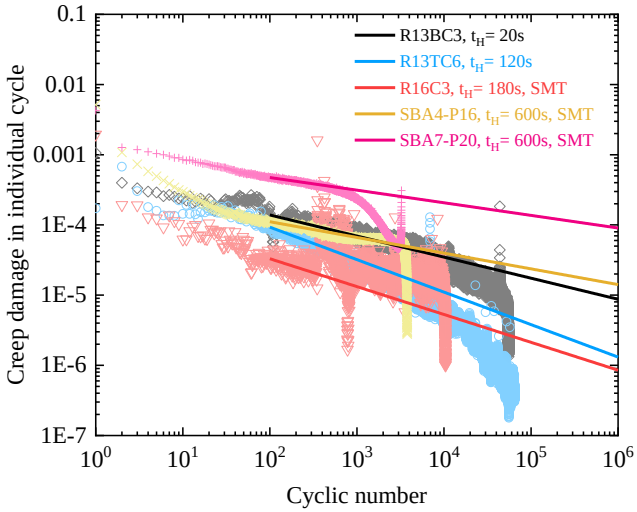

(a)

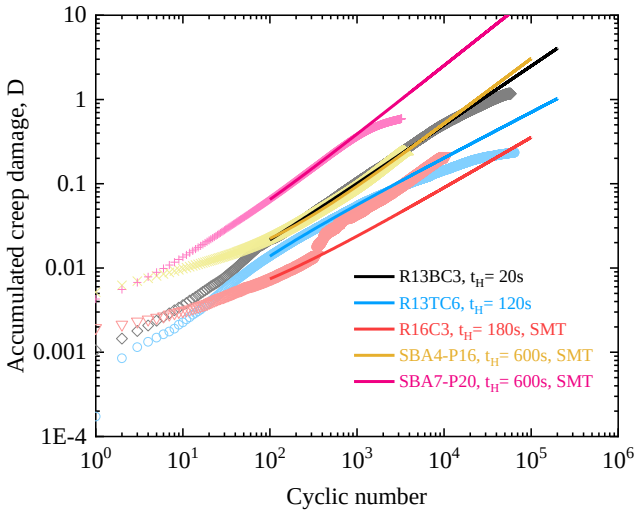

(b)

Figure 12. (a) Extrapolation in creep damage increment and (b) the accumulated creep damage calculated based on the extrapolation as a function of the applied cycles.

Using the lower bound of 0.2 for the creep damage accumulation described previously, the CF life is predicted for the CF cycles at the total accumulated creep damage of 0.2. The results are summarized in Table 4. The experimental cycles for the accumulated creep damage of 0.2 and the failure cycles are also listed in Table 4 for comparison. Except for the Type 1 SMT R16C3 in which multiple interruptions occurred, it is conservative to use the lower bound of the predicted cycles at 0.2 accumulated creep damage as the predicted CF failure cycles.

It is also noted that calculated accumulated creep damage from all the cycles prior to failure ranges from 0.21 to 1.16 for these 5 tests. There are factors that needs mentioning for this approach. First, the LMP relationship for the creep rupture time is for average behavior. In reality, there are test data variations in both creep rupture life and CF life cycles, and both would explain the variation in the calculated creep damage. Second, the assumption of the creep damage approach is that the low strain range CF life calycles are dominated by creep damage, however, 4 data points have accumulated creep damage calculated to be less than 0.6, thus, there are additional factors that needs to be explored in using this approach, which is beyond the scope of this report.

Table 4. Results of CF life prediction using creep damage accumulation method.

Specimen ID	Predicted cycles with accumulated creep damage of 0.2	Experimental cycles with accumulated creep damage of 0.2	Experimental cycles to failure	Accumulated creep damage of all experimental cycles
R13BC3	2,690	2,584	55,289	1.17
R13TC6	9,830	25,966	64,659	0.23
R16C3	38,430	9,255	10,766	0.21
SBA4-P16	2,840	2,759	3,641	0.25
SBA7-P20	440	441	3,224	0.59

4.2 DISSIPATED WORK-BASED METHOD

4.2.1 Dissipated Work Calculation of CF Tests

An alternative method evaluated in the current report is the dissipated work -based approach in which the basic assumption is that the CF life cycles is determined by the total work dissipated in the test specimen during the CF deformation. The illustration of the dissipated work, *W*, in one hysteresis loop is presented in Figure 13.

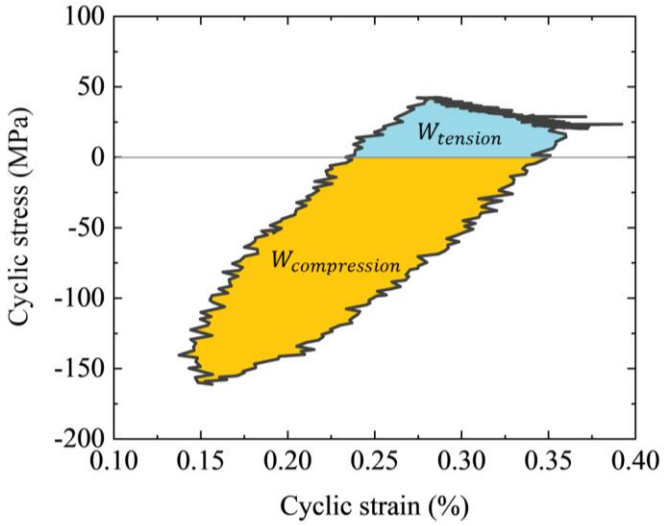

Figure 13. Illustration of the dissipation work in one hysteresis loop.

The dissipated work, W, is expressed as:

$$W = W_{tension} + W_{compression} = \int \sigma_{tension} d\varepsilon + \int \sigma_{compression} d\varepsilon, \quad (6)$$

where $W_{tension}$ and $W_{compression}$ are the dissipated work from tensile load and compressive load, respectively; $\sigma_{tension}$ and $\sigma_{compression}$ are the tensile and compressive stresses; and ε is the cyclic strain.

4.2.2 Dissipated Work Calculation and CF Life Prediction at Low Strain Ranges

The dissipated work of each cycle and the accumulated dissipated work as a function of applied cycles are presented in Figure 14 for R13BC3 and R13TC6, in Figure 14 for R16C3, and in Figure 16 for SBA4-P16 and SBA7-P20. The linear trend line curves in a log-log scale of the accumulated dissipated work by using the values from 100–200 cycles are also presented in the figures, except for R13BC3 in which the data showed discontinuities at these cycles due to test interruptions. The accumulated dissipated work at failure for these data is in the 380–2,000 mJ/mm^3 range.

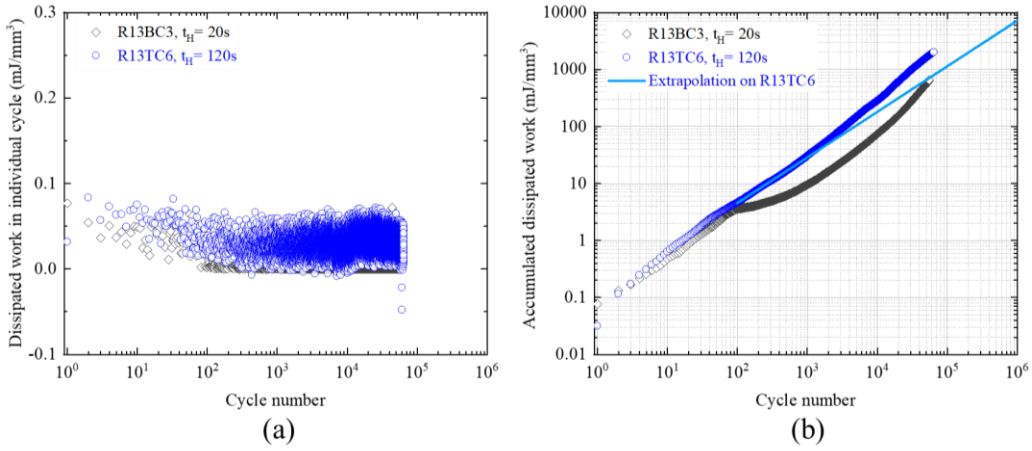

Figure 14. (a) Dissipated work of each cycle and (b) the accumulated Dissipated work as a function of applied cycles for R13BC3 and R13TC6.

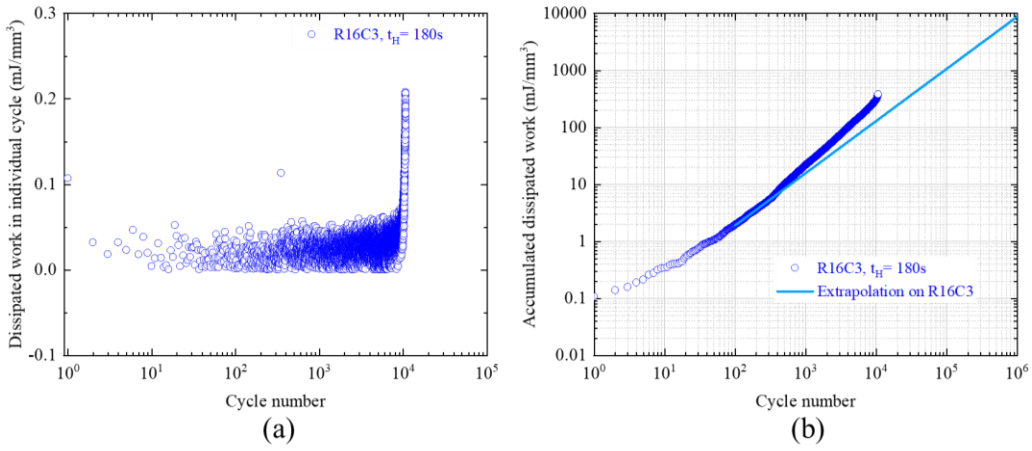

Figure 15. (a) Dissipated work of each cycle and (b) the accumulated dissipated work as a function of applied cycles for R16C3

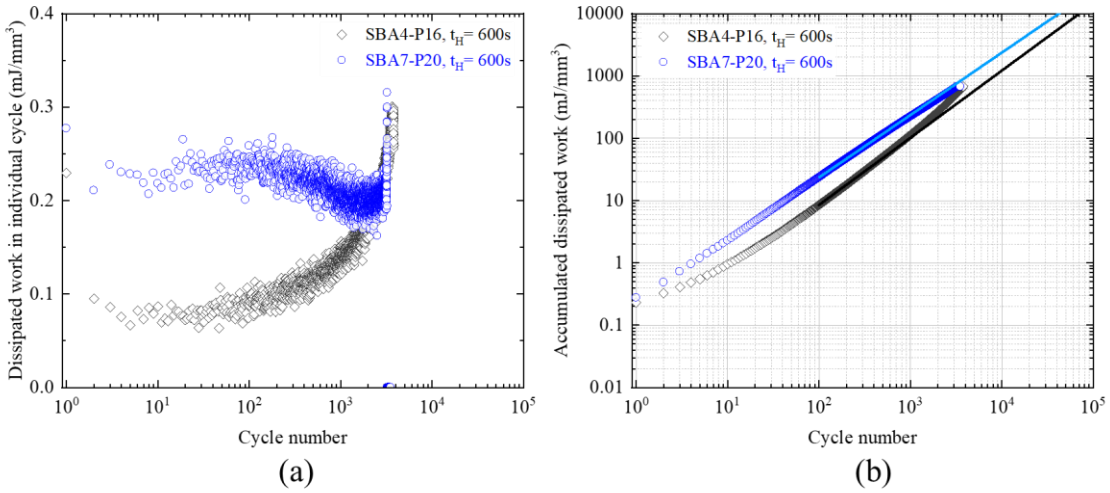

Figure 16. (a) Dissipated work of each cycle and (b) the accumulated dissipated work as a function of applied cycles for SBA4-P16 and SBA7-P20.

Alternatively, according to Ostergen's model for the CF life prediction (Ostergen 1976), the damage accumulated in the specimen to cause failure is determined by the accumulated net tensile part of dissipated work of all the applied cycles (i.e., the summation of the blue portion of the area shown in Figure 13). The argument is that that the tensile stresses are believed to induce the creep voids and thus propagate cracks to cause failure. In this study, the net tensile dissipation work is analyzed, and the results are presented in Figure 17 for R13BC3 and R13TC6, in Figure 18 for R16C3, and in Figure 19 for SBA4-P16 and SBA7-P20. The linear trend line curves in a log-log scale of the accumulated tensile dissipated work by using the values from 100 to 200 cycles are also presented in the figures. The amount of tensile dissipated work accumulated to cause failure in these tests are range from 150 to 590 mJ/mm^3.

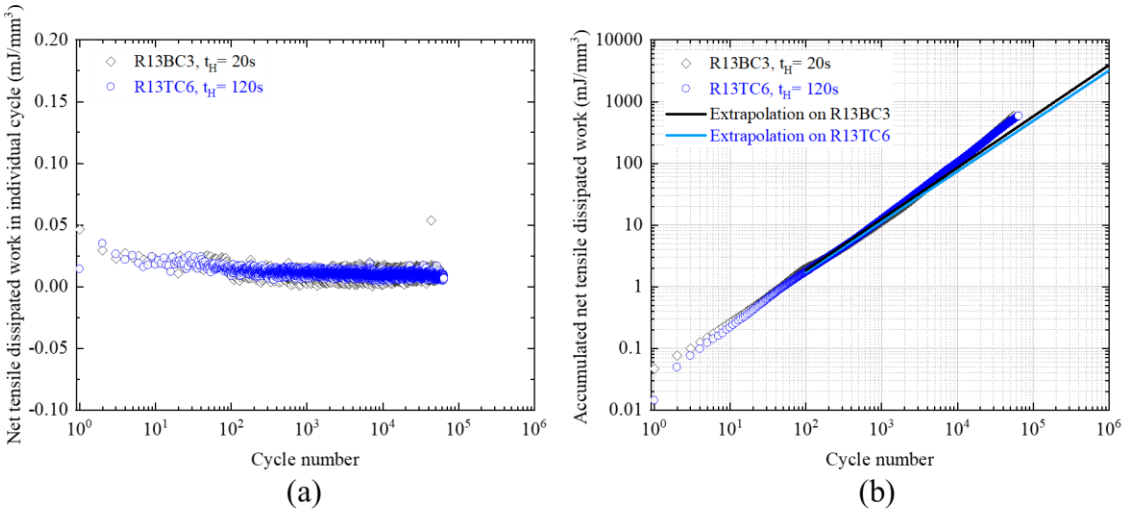

Figure 17. (a) Tensile dissipated work of each cycle and (b) the accumulated tensile dissipated work as a function of applied cycles for R13BC3 and R13TC6.

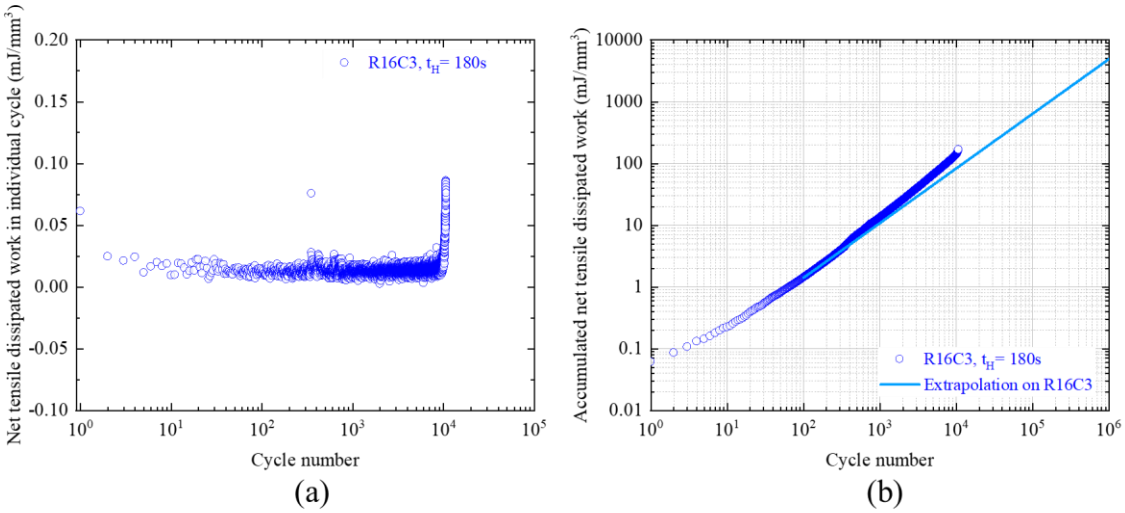

Figure 18. (a) Tensile dissipated work of each cycle and (b) the accumulated tensile dissipated work as a function of applied cycles for R16C3.

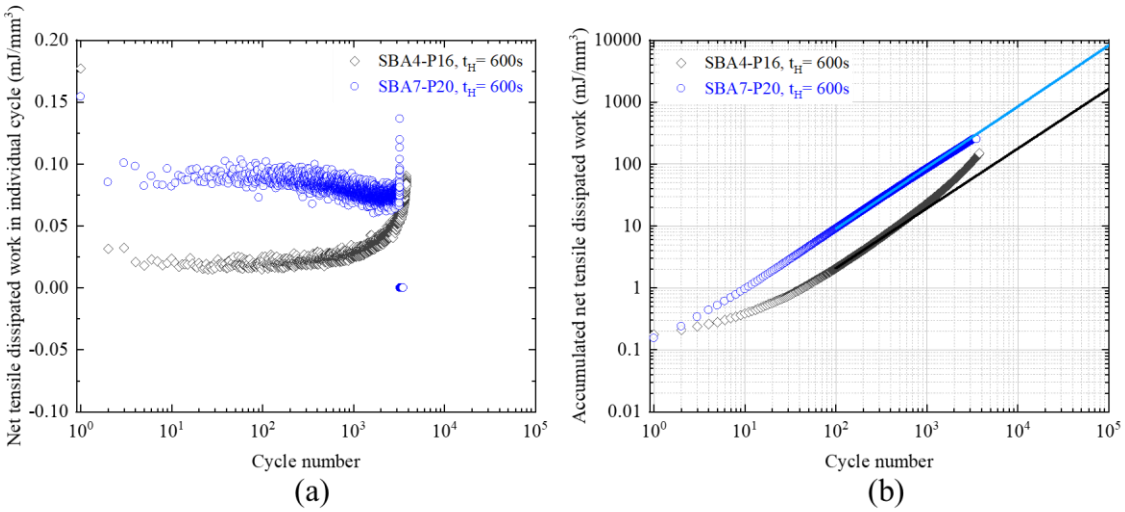

Figure 19. (a) Tensile dissipated work of each cycle and (b) the accumulated tensile dissipated work as a function of applied cycles for SBA4-P16 and SBA7-P20.

To develop a conservative design approximation on the CF life, the low-bound value of 380 mJ/m^3 for total accumulated dissipated work and 150 mJ/mm^3 for the accumulated tensile dissipated work were selected as criteria in identifying the predicted CF cycles to failure, and the results are summarized in Table 5. Again, except for two cases—the Type 1 SMT R16C3 where multiple interruptions occurred and SBA4-P16 with too large elastic follow-up factors of 6—the predicted CF failure cycles based on lower bound of the dissipated work are conservative, and these two work-based methods showed insignificant deference in the predicted CF life cycles.

Table 5. Results of CF life cycles predicted using total dissipated work and tensile dissipated work methods.

Specimen ID	Total work at fracture (mJ/mm^3)	Net tensile work at fracture (mJ/mm^3)	Predicted cycles to failure using total work of 240 mJ/mm^3	Predicted cycles to failure using tensile work of 150 mJ/mm^3	Experimental cycles to failure
R13BC3	655	586	-	19,966	55,289
R13TC6	2,002	586	25,609	23,898	64,659
R16C3	381	168	32,397	19,421	10,766
SBA4-P16	637	151	3,400	8,470	3,780
SBA7-P20	677	252	1,624	1,781	3,250

4.3 COMPARISON OF CF CYCLES USING DIFFERENT EXTRAPOLATION METHODS

A comparison of the predicted CF life cycles using creep damage accumulation, total dissipated work , and net tensile dissipated work methods is presented in Figure 20 for the five available CF failure data at low strain ranges. In the figure, envelopes of such a relationship between the predicted CF life cycles, $N_{f.predicted}$, with experimental observed cycles, $N_{f.experimental}$, as

$$N_{f.predicted} = F * N_{f.experimental} \tag{7}$$

where *F* is an applied factor. In this figure, the dashed line with *F=1* represents the case where the predicted life cycles equal to the experimental cycles to failure. In addition, the envelopes with *F=0.5, 2, 0.05* and 20 are also presented. For the data points below *F=1*, the predicted CF life cycles are conservative.

Overall, the creep damage accumulation method generates deviation further away experimental observed CF cycles to failure, comparing with the total dissipated work and net tensile dissipated work methods because multiple points predicted with creep damage accumulation method fall further outside the *F=2* line. The predictions between two dissipated work-based methods show very similar results and within the *F=2* and *F=0.5* envelopes. These preliminary results indicate that the work-based CF life prediction method is more accurate.

It is noted that the analysis was conducted on a limited number of specimens with test temperature only at 950°C and with relatively short hold times. The assessment on these methods for predicting CF life cycles with the effect of hold time and temperature needs further investigation.

In the Section 5 below, an experimental method is proposed to generate the information necessary for developing the CF design curves at low strain ranges based on the CF life cycles predicted using the dissipated work-based method. Several cases were evaluated using the tensile dissipated work method, but the noises in the data, especially for those cases with very small strain ranges of <0.1%, caused inconsistent results. The analysis below was focused on total dissipated work-based method.

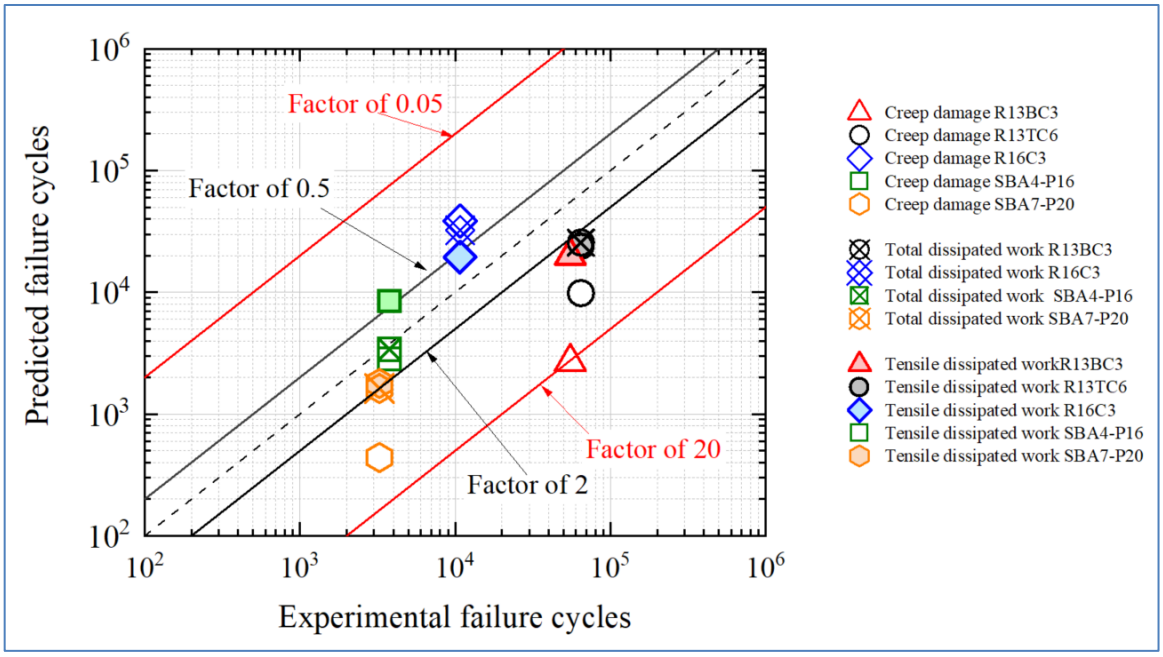

Figure 20. CF life cycles prediction using creep damage accumulation, total dissipated work, and net tensile dissipated work methods on Alloy 617 subjected to low strain range CF at 950°C.

5. TESTING IN GENERATING CF DESIGN CURVES AT LOW STRAIN RANGES

Two types of experimental data are needed to support generating the CF design curves at low strain ranges. First, standard CF with different strain ranges and hold times can be used with a limited number of cycles to provide necessary information in predicting the CF cycles. CF design curves can be developed by using the predicted life cycles. Second, there must be experimental data points to verify the proposed design curves.

5.1 BLOCK STRAIN RANGE CF TESTING

The aforementioned analysis shows that standard CF testing with a limited number of cycles would provide the necessary information needed to predict its CF life cycles through trend line extrapolation by using the work-based life cycle prediction method described in the previous section. A series of strain-controlled standard CF testing on a single specimen is designed, and the test is performed with blocks of CF loading profiles. Each block of the CF test has one set of parameters (i.e., a pre-described strain range and the tension hold time). One example of this type of testing on specimen R12BC6-2106 is ongoing at 950°C, and the testing parameters are listed in Table 6. This block strain range CF testing method significantly reduces the testing time and provides critical information needed to develop the CF design curves at low strain ranges.

It is noted that this block strain range CF concept assumes the loading history has no effect in the dissipated work-based prediction of CF life cycles. This assumption is based on experience and needs to be verified. A simple approach for the verification procedure is to insert these CF blocks at a later stage of the testing. If the predicted CF life cycles are comparable between the beginning blocks and the blocks at the later stage with the same testing parameter, the loading history effect is negligible.

Table 6. Block strain range CF at 950°C and results of predicted CF life cycles

Block ID	Nominal strain range (%)	Tension hold time (s)	Predicted cycles to failure
1	0.17	100	8,185
2	0.15	100	7,462
3	0.13	100	49,619
4	0.09	100	119,377
5	0.07	100	7,352,265
6	0.17	1,000	TBD
7	0.15	1,000	TBD
8	0.13	1,000	TBD
9	0.09	1,000	TBD
10	0.07	1,000	TBD
11	TBD	TBD	TBD

The first five blocks of the CF cycles were completed, and the maximum and minimum stresses and strain ranges are plotted in Figure 21.. The dissipated work was calculated for the tested CF cycles of each block. The total dissipated work in each cycle and accumulated dissipated work as a function of applied cycle are presented in Figure 22. As expected, the noise in the data is large. The extrapolation trend lines generated by using the linear portion in the dissipated work accumulation are also presented in Figure 22. The value of 380 mJ/mm^3 bounding value in work accumulation is then used to identify the predicted CF failure cycles. The predicted CF cycles to failure for each block of strain ranges are also listed in Table 6.

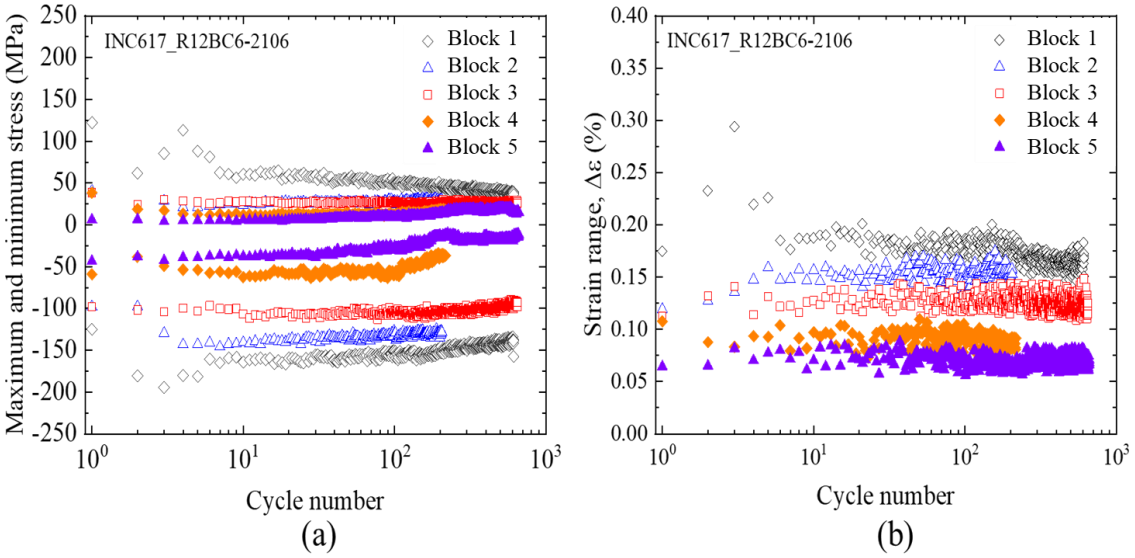

Figure 21. (a) Maximum and minimum stresses and (b) strain ranges as a function of applied cycles for the first five blocks of CF cycles.

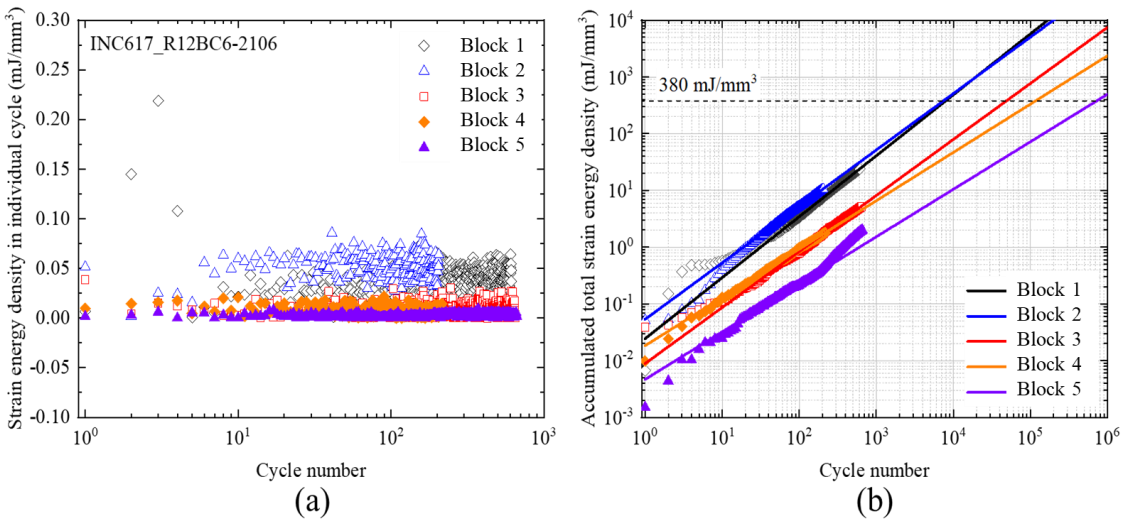

Figure 22. (a) Dissipated work in each cycle and (b) the accumulated dissipated work as a function of applied cycles for the block strain range CF test.

5.2 PRELIMINARY CF DESIGN CURVES

The method of deciding the best fit curve for CF life cycles at high strain ranges (i.e., strain ranges at 0.3% or higher) was described in Messner et al. (2018) and Wang et al. (2020a). A preliminary best fit curve for the CF life cycle with the hold time of 100 s is generated by connecting the curve from the high strain range region to the curve from the low strain range region. The low strain range curve was based on the predicted CF life cycles shown in Table 6. The results are presented in Figure 23.

The preliminary CF design curve with a tension hold time of 100 s is then generated by the conventional method (i.e., the lesser of the two curves when a reduction factor of 2 on the strain range and a reduction factor of 20 on the number of cycles to failure are applied to the best-fit curve). For comparison, the ASME fatigue design curve at 950°C and the best-fit pure fatigue curve are also plotted in Figure 23.

The concept of developing additional CF design curves with longer hold times will require additional block strain range testing with longer hold times. This is the reason for additional designed block strain range test conditions listed as block 6 to block 11 in Table 6. When multiple hold time test conditions are completed and the predicted CF life cycles are generated, an extrapolation method for determining the CF life cycles with longer hold time can be developed.

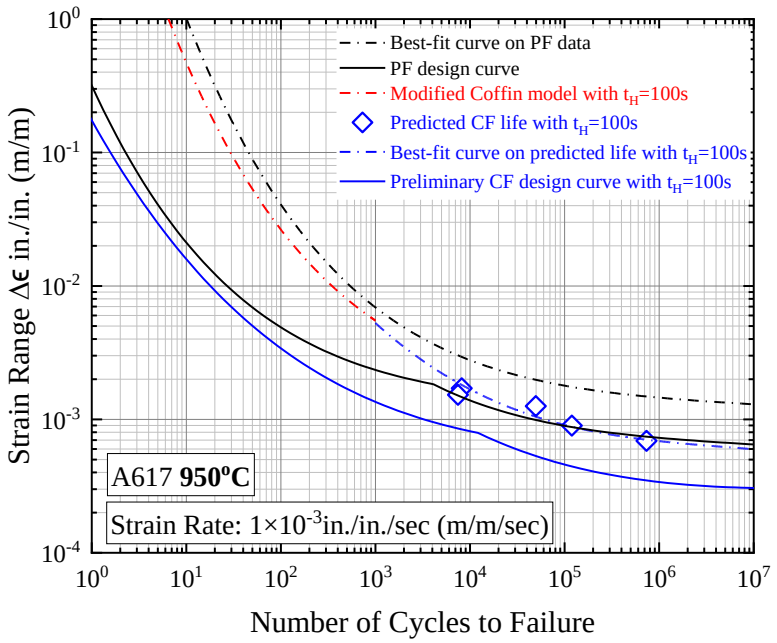

Figure 23. Preliminary CF design curve for Alloy 617 at 950°C with the hold time of 100 s

5.3 EXPERIMENTS IN VALIDATING THE CF DESGIN CURVE

Additional experimental data are needed to validate the CF design curve at low strain ranges. As previously discussed, it is impractical to perform standard strain-controlled CF tests to obtain failure data. However, one can take advantage of CF tests with elastic follow-up (i.e., SMT-based CF testing). Because of the enhanced creep damage for SMT-based CF tests, the failure cycles are significantly reduced and thus testing duration is reasonable.

Two SMT-based tests designed at low strain ranges are listed in Table 7. A617-P10 had a nominal elastic follow-up factor of 4.0 and was tested for 37,693 cycles with an initial stable strain range of 0.125%. This test was interrupted without failure. R12TC4-05 is ongoing using the SBSMT test method on a standard CF specimen. The initial test strain range is 0.2% for R12TC4-05 and has accumulated more than 3,000 cycles at the time of this reporting. Both tests have a tension hold time of 600 s.

Table 7. SMT-based CF testing for Alloy 617 at 950°C.

Test ID	Testing type	Specimen geometry	Initial stable strain range (%)	Elastic follow-up factor	Tension hold time (s)	Cycles to failure
A617-P10[1)]	Original Tubular SMT[1]	Tubular SMT specimen with internal pressure of 150 psi	0.125	4	600	Interrupted at 37,693 cycles
R12TC4-05[2)]	SBSMT[2]	Standard CF specimen	0.18	3	600	Ongoing

[1] The testing method was described in Wang et al. (2017a).
[2] The testing method was described in Wang et al. (2019).

The available measured cycles of these two tests were used to calculate the dissipated work, and the results of the accumulated dissipated work are presented in Figure 24 . The calculated dissipation work accumulated from 100 to 200 cycles were then used to obtain the linear extrapolation curves. The extrapolation is in good agreement with the measured data for both tests. Using the same lower bound value for accumulated dissipated work of 380 mJ/mm^3, the predicted CF life cycles are 21,102 for A617-P10 and 5,517 for R12TC4-05. Because the predicted CF life cycles for A617-P10 are less than the experimental accumulated cycles, this test has validated that the dissipated work -based CF life prediction method is conservative. The test on R12TC4-05 is planned to continue until failure to provide a second validation data point.

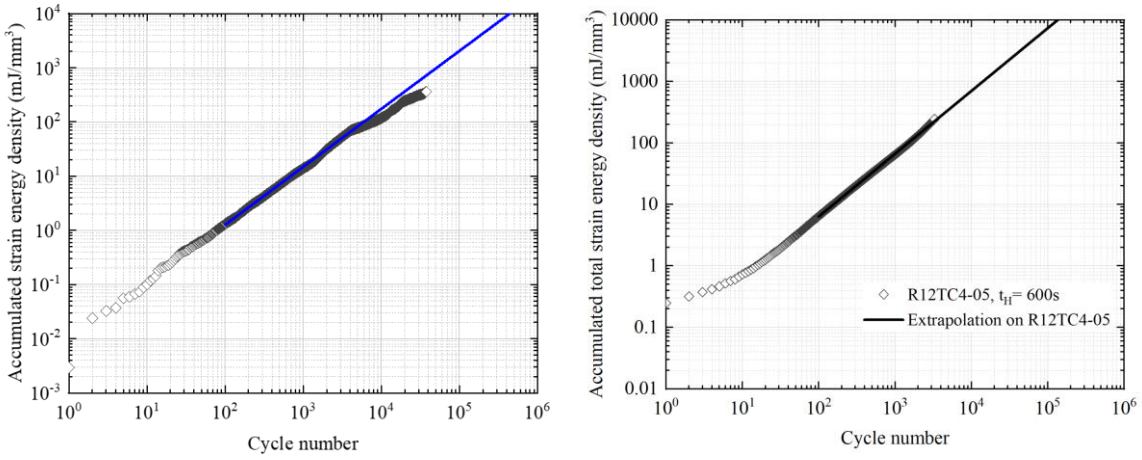

(a) (b)

Figure 24. Accumulated dissipated work as a function of applied cycles for (a) P10-10 and (b) R12TC4-05 along with the linear extrapolation curves.

6. SUMMARY

The lack of test data in the high cycle and low strain range region is a critical issue in finalizing the EPP+SMT CF design curves. The limitations in experimental data at low strain ranges and long hold times are due to extraordinarily long failure times at the small strain ranges and the inability of the test machine to control these small strain ranges because of the signal to noise issues.

In this work, available CF data with failure cycles at strain ranges less than 0.3% were analyzed and used to assess two methods in predicting the CF life cycles: the accumulated creep damage-based method and dissipated work -based method. The results indicate that it is possible to use a limited number of testing cycles to predict the CF life cycles via a simple extrapolation method.

Experiments with the concept of proposed block-strain range CF testing method were designed by using standard strain-controlled CF in generating the critical information needed to predict CF life cycles. Based on this new testing approach, a preliminary EPP+SMT CF design curve was developed for Alloy 617 at 950°C with a tension hold time of 100 s. Additional tests are ongoing, and the goal is to produce information regarding the extrapolation of the longer hold time effect within a reasonable amount of time and testing effort.

Additionally, SMT-based tests were designed and being performed to validate EPP+SMT CF design fatigue curves generated using the predicted CF life cycles. Critical testing in support of finalizing the EPP+SMT CF design curves will continue in FY22.

REFERENCES

ASMT E2714, *"Standard Test Method for Creep-Fatigue Testing",* ASTM International, West Conshohocken, PA.

ASTM-E606, *"Standard Test Method for Strain-Controlled Fatigue Testing"*, ASTM International, West Conshohocken, PA.

Barua, B, Messner, M.C., Sham, T.-L., Jetter, R. I., Wang, Y., (2020), *"Preliminary description of a new creep-fatigue design method that reduces over conservatism and simplifies the high temperature design process"*, ANL-ART-194, Argonne National Laboratory, Lemont, IL.

Barua, B, Messner, M.C., Wang, Y., Sham, T.-L., Jetter, R. I. (2021), *"Draft Rules for Alloy 617 Creep-Fatigue Design using an EPP+SMT Approach"*, ANL-ART-227, Argonne National Laboratory, Lemont, IL

Hales, R.,(1980), "*A Quantitative Metallographic Assessment of Structural Degradation of Type 316 Stainless Steel during Creep-Fatigue*", Vol. 3, No. 4, pp. 339-356, Fatigue of Engineering Materials and Structures.

Manson, S. S. and Zab, R.,, (1977), "*Treatment of Low Strains and Long Hold Times in High Temperature Metal Fatigue by Strain Range Partitioning*", ORNL/sub-3988/1, Oak Ridge National Laboratory, Oak Ridge, TN.

Messner, M. C., Sham, T. L., Wang, Y., and R. I. Jetter, R.I. (2018), *"Evaluation of methods to determine strain ranges for use in SMT design curves"*, ANL-ART-138, Argonne National Laboratory, Lemont, IL.

Ostergren, W. J. "*A damage function and associated failure equations for predicting hold time and frequency effects in elevated temperature, low cycle fatigue*", Journal of Testing and Evaluation 4.5 (1976): 327-339.

Wang, Y., Jetter, R. I., Krishnan, K., and Sham, T.-L (2013) *"Progress Report on Creep-Fatigue Design Method Development Based on SMT Approach for Alloy 617"*, ORNL/TM-2013/349, Oak Ridge National Laboratory, Oak Ridge, TN.

Wang, Y., Jetter, R. I. and Sham, T.-L (2014), *"Application of Combined Sustained and Cyclic Loading Test Results to Alloy 617 Elevated Temperature Design Criteria"*, ORNL/TM-2014/294, Oak Ridge National Laboratory, Oak Ridge, TN.

Wang, Y., Jetter, R. I., Baird, S. T., Pu, C. and Sham, T.-L. (2015), *"Report on FY15 Two-Bar Thermal Ratcheting Test Results"*, ORNL/TM-2015/284, Oak Ridge National Laboratory, Oak Ridge, TN.

Wang, Y., Jetter, R. I., and Sham, T.-L. (2016a), "FY16 Progress Report on Test Results In Support Of Integrated EPP and SMT Design Methods Development" ORNL/TM-2016/330, Oak Ridge National Laboratory, Oak Ridge, TN.

Wang, Y., Jetter, R. I., and Sham, T.-L. (2016b), *"Preliminary Test Results in Support of Integrated EPP and SMT Design Methods Development"*, ORNL/TM-2016/76, Oak Ridge National Laboratory, Oak Ridge, TN.

Wang, Y., Jetter, R.I., and Sham, T.-L. (2017a), *"Report on FY17 Testing in Support of Integrated EPP-SMT Design Methods Development"*, ORNL/TM-2017/351, Oak Ridge National Laboratory, Oak Ridge, TN.

Wang, Y., Jetter, and Sham, T.-L. (2017b), *"Pressurized Creep-Fatigue Testing of Alloy 617 Using Simplified Model Test Method",* Proceedings of the ASME 2017 Pressure Vessels and Piping Conference, PVP2017-65457, American Society of Mechanical Engineers, New York, NY.

Wang, Y., Jetter, R. I., Messner, M., Mohanty, S., and Sham, T.-L. (2017c), *"Combined Load and Displacement Controlled Testing to Support Development of Simplified Component Design Rules for Elevated Temperature Service"*, Proceedings of the ASME 2017 Pressure Vessels and Piping Conference, PVP2017-65455, American Society of Mechanical Engineers, New York, NY.

Wright, J. K., et al. "*Determination of the creep-fatigue interaction diagram for Alloy 617*", Pressure Vessels and Piping Conference. Vol. 50411. American Society of Mechanical Engineers, 2016.

Wang, Y., Jetter, R. I., Messner, M., and Sham, T.-L. (2018), *"Report on FY18 Testing Results in Support of Integrated EPP-SMT Design Methods Development"*, ORNL/TM-2018/887, Oak Ridge National Laboratory, Oak Ridge, TN.

Wang, Y., Jetter, R. I., Messner, M., and Sham, T.-L. (2019), *"Development of Simplified Model Test Method for Creep-fatigue Evaluation"*, Proceedings of the ASME 2019 Pressure Vessels and Piping Conference, PVP2019-93648, American Society of Mechanical Engineers, New York, NY.

Wang, Y., Hou, P., Jetter, R. I., and Sham, T.-L. (2020), *"Report on FY2020 Test Results in Support of the Development of EPP Plus SMT Design Method"*, ORNL/TM-2020/1620, Oak Ridge National Laboratory, Oak Ridge, TN.

Wang, Y., Hou, P., Jetter, R. I., and Sham, T.-L. (2021), *"Evaluation of the Primary-Load Effects on Creep-Fatigue Life of Alloy 617 Using Simplified Model Test Method"*, Proceedings of the ASME 2021 Pressure Vessels and Piping Conference, PVP2021-61658, American Society of Mechanical Engineers, New York, NY